ISSN: 0067-2904

Study of Optical, Structural and Morphology Properties of Tin Oxide Nanoparticles by Pulse Laser Ablation and its Effect on Bacteria *Staphylococcus aureus*

Zahraa A. Saeed , Kadhim A. Aadim*
Department of Physics, College of Science, University of Baghdad, Baghdad, Iraq

Received: 5/6/2022 Accepted: 10/12/2022 Published: 30/11/2023

Abstract

Tin oxide (Sn) nanoparticles were prepared by pulsed laser ablation (PLA) method at different laser energies (400-700mJ). (UV, XRD, AFM, SEM, EDS) methods were employed to determine the properties of nanomaterials. The optical properties showed that the energy gap decreased with increasing laser power; the structural properties showed the relationship between density and angle; Miller's coefficients for net angles were determined and the morphology properties showed the element's surface shape and surface roughness. Also, Tin oxide nanoparticles with added to *Staphylococcus aureus* bacteria isolated from the ear and cultured by striking method on nutrient agar to know the effect of tin oxide nanoparticles on the growth of this bacteria. The results showed that tin (Sn) oxide nanoparticles had a role in decreasing the growth of bacteria on cultured media using the laser energies of (400mJ, 500mJ and 600mJ), but at an energy of 700mJ a clear zone (no growth) of bacteria on cultured media was noted, indicating 100% bacterial killing.

Keywords: Pulse laser ablation (PLA), Nanoparticles (NPs), Tin (Sn) oxide, *Staphylococcus aureus* bacteria.

دراسة الخصائص البصرية والهيكلية والتشكيلية لجسيمات أكسيد القصدير النانوية بواسطة الاستئصال بالليزر النبضي وتأثيره على بكتيريا المكورات العنقودية الذهبية

زهراء عبدالكريم سعيد ، كاظم عبدالواحد عادم*
قسم الفيزياء، كلية العلوم، جامعة بغداد، بغداد، العراق

الخلاصة

تم تحضير الجيسمات النانوية من القصدير بطريقة الاستئصال بالليزر النبضي عند طاقات ليزر مختلفة ، وتم فحص هذه المادة بواسطة (الخصائص البصرية ، الخصائص التركيبية ، الخصائص التشكيلية) لمعرفة خصائص المواد النانوية. اظهرت الخصائص البصرية ان فجوة الطاقة تتناقص مع زيادة طاقة الليزر ، والخصائص التركيبية اظهرت العلاقة بين الكثافة والزاوية وتم تحديد معاملات ملر للزوايا الواضحة ، واظهرت الخصائص التشكيلية شكل سطح العنصر وخشونة السطح. تم أضافة جزيئات الأوكسيد النانوية مع بكتيريا المكورات العنقودية الذهبية، المعزولة من الأذن والمزروعة بطريقة التخطيط على الوسط المغذي، لمعرفة تأثير المواد النانوية على نمو هذه البكتيريا. اظهرت النتائج ان الجسيمات النانوية لأوكسيد القصدير كان لها دور في انخفاض نمو البكتيريا على الوسط الزرعي عند استخدام الطاقات (400 ، 500 ، 600 ملي جول) ، ولكن

*Email: kadhim_adem@scbaghdad.edu.iq

عند الطاقة 700 ملي جول ظهرت منطقة (لايوجد نمو) للبكتيريا على الوسط الزرعي ،حيث كانت نتيجة القتل 100%.

I. Introduction.

Recently, short pulse laser-matter interaction (LMI) has attracted much attention because pulsed laser technologies have expanded laser-driven material processing and research capabilities. Examples include advancements in high-precision cutting and drilling [1], surface nanostructuring [2], nanoparticle synthesis [3] and laser-induced plasma spectroscopy[4].

Pulse laser ablation (PLA) is a laser-induced ejection of macroscopic volumes of material from the surface of a solid. Short, intense laser pulses are used, and the process is known as laser ejection process; it is not widely used despite its prevalence in many technology sectors [5]. Laser ablation technology is defined as removing matter from the surface of a target through strong laser irradiation. The laser causes electrons from the conduction band in metals to condense by heating them to high temperatures. As depicted in Figure 1, the heated electron gas excites phonons in the lattice and equilibrates on a picosecond timescale, resulting in a state of equilibrium.

The purpose of this research is to examine the changes that occur when a second laser pulse reaches the target with a different time delay than the first laser pulse [6]. In this work, what happens when a second laser pulse hits the target at a different time delay than the first laser pulse was inestigated. Also, how the process is altered as a result was studied. It is possible to emit a plume of particles into the surrounding environment during the ablation process, including ions, neutral atoms, and bigger fragments. Because of this, laser ablation can be used to fabricate nanoparticles (NPs) and produce thin films and other applications. [7].

Nanotechnology is a promising tool in several research disciplines, including pharmaceuticals, diagnostics, the environment, information technology, engineering, the energy industry, electronics, and the chemical industry. Nanomaterials exhibit new physical and chemical properties connected with their "nano-scale" structure. As a result of the unique qualities of nanomaterials, there is a tremendous opportunity for the production of various products with differentiated purposes. These distinct characteristics include size, shape, surface properties, aggregation state, solubility, structure, and chemical composition. Because of their chemical stability, biocompatibility, and low toxicity, selenium and tin nanoparticles have gained considerable attention for their synthesis and application [8].

Staphylococcus aureus is a gram-positive opportunistic pathogen with virulence characteristics that have emerged in the environment. One of the essential functions of this network of virulence factors is to detect changes in the environment and respond by altering the production of virulence factors required for survival in the host, such as cell surface adhesives, enzymes, and extracellular toxins order to maintain survival in the host. [9].

II. Materials and methods.

1. Synthesis of Sn nanoparticles.

This work was pressing (2g) of tin (Sn) micro powder was pressed into a solid disc with a hydraulic press. The solid circular disc of 1cm in diameter was placed in a small beaker, to which 4 mL of distilled water was added to cover the solid disc. The beaker was placed on the base of the laser holder, and the pulse laser with a wavelength of 1064 nm 200 shoots was

projected to the target (Tin disc) with different laser energy (400-700mJ), as in Figure (1). A change in the color of the distilled water was noticed due to the laser's interaction with the target, indicating the formation of the nanomaterial.

2. Treatment of Staphylococcus aureus bacteria.

The solid disc of the Sn target was placed in a beaker. And add the best serial dilution 10^{-7} of *Staphylococcus aureus* until it completely covers the solid disc and then bombarded by lasers with different energy 400, 500, 600, and 700 mJ. The liquid from the ablation was added to the plain tube, and cultivated on nutrient agar using the striking method.

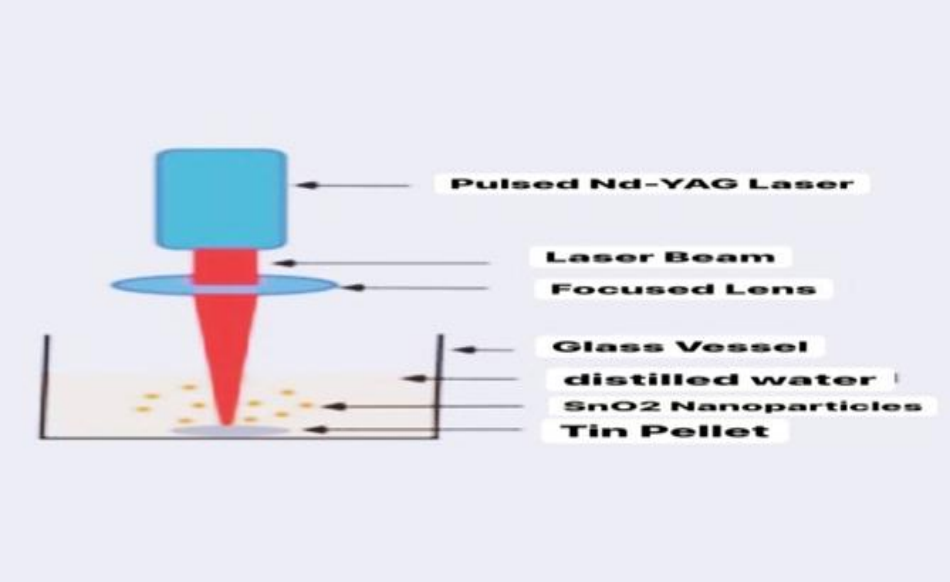

Figure 1: : Schematic diagram of pulsed laser ablation in a liquid system.

III.Result and Discussion.

1. X-ray Diffraction Analysis (XRD)

This technique gives information about the structural properties of the nanoparticles. This technique characterizes crystal structure and calculates their crystalline size through the Scherrer's equation, as equation (1):

$$D = 0.9\lambda / B(\cos \theta_B) \quad \ldots\ldots (1)$$

Where λ is the wavelength, B is the full width at half maximum (FWHM) of the peak, and θ_B is the Bragg angle [10]. Figure 2a shows the X-ray diffraction pattern of pureTin (Sn), where clear peaks appeared at diffraction angles (2θº) 30.58, 31.96, 44.10, 45.10, 55.54, 62.72, 63.94, 64.78, 72.60, 73.93 and 79.68, corresponding to (200), (101), (220), (211), (301), (112), (400), (321), (420) and (411) planes,respectively. Its average crystal size (86.1400518nm), as deduced from Figure (2a). These results are in complete agreement with the standard model (JCPDS data card no.: 00-004-0673) for pure face-centred cubic phase Tin (Sn) nanoparticles. This result agrees with that of Shadangi et al.[11]. Figure 2b shows the X-ray diffraction of Tin (Sn) oxide nanoparticles.Several peaks located at 2Θ° ranging from 10° to 80°, With cell parameters 21.6, 37.8, 44.76, 55.66 and 62.306, corresponding to the Miller coefficients (111), (220), (311), (400), (331) respectively. Its average crystal size (24.061822nm),whose locations correspond to ICC datacard No. 00-005-0390 in the XRD pattern of Tin (Sn) oxide [12].

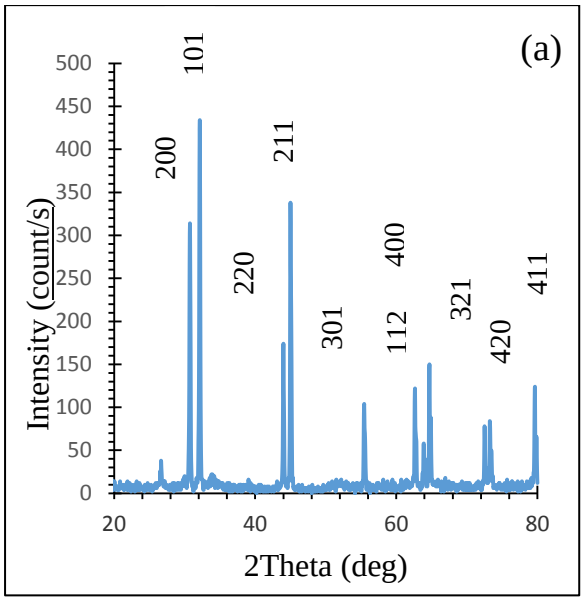

Figure 2a: shows the X-ray diffraction of the Tin (Sn) powder.

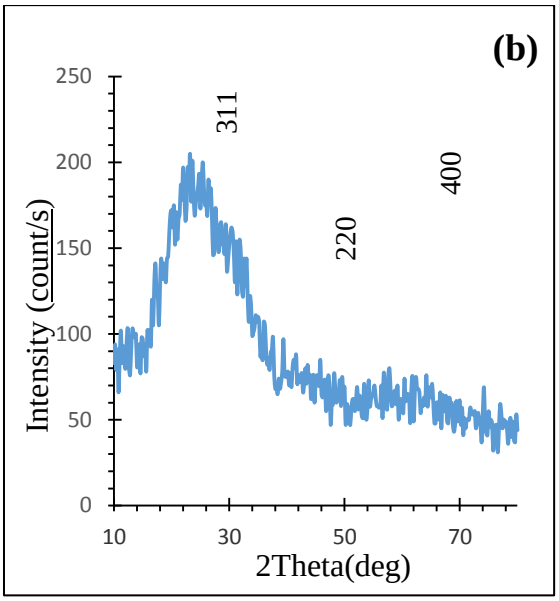

Figure 2b: shows the X-ray diffraction of theTin (Sn) oxide nanoparticles.

2. Ultraviolet-Visible Spectroscopy analysis (UV-Visible)

It is a technique used for fast analysis; it measures the transmittance or absorbance of light [13]. Figure 3 shows the optical absorption spectra of tin (Sn) oxide nanoparticles at different laser energies (400-700 mJ), which were located in the wavelength range of (288-296) nm. Based of the absorbance spectra, the tin (Sn) oxide nanoparticles' absorption coefficients were determined graphically by applying Tauc's formula for direct transition, as shown in formula (2):

$$(\alpha h\nu) = B(h\nu - E_{opt})^{r} \quad \ldots\ldots (2)$$

Where: E_{opt} is the optical energy gap, B is a constant which depends on material structure and r is an index which can be assumed to have values of 1/2, 3/2, 2 and 3, depending on the nature of the electronic transition responsible for the absorption. Also, r = 1/2 for allowed direct transition, r = 3/2 for forbidden direct transition and r = 3 for forbidden indirect transition, with r = 2 refers to indirect allowed transitions [14].

Plotting of the relationship of (hυ) versus $(\alpha h\upsilon)^{1/2}$ and obtaining an extrapolation line of the linear relationship is a common method for measuring the bandgap, as shown in Figure 4. The bandgap energies reported in Table 1 show that the energy gap decreases with the increase of the laser energy. This decrease in the energy gap is caused by an increase in the granular size of the material, which creates donor levels within the energy gap and near the conduction band and thus increases the absorption of photons of less energy. This result is consistent with the results of Mahmood et al.[15] .

Table 1: The energy gap that varies with the change in laser energy.

Laser energy (mJ)	Bandgap energy (eV)
400	3.3
500	3.2
600	3.1
700	3

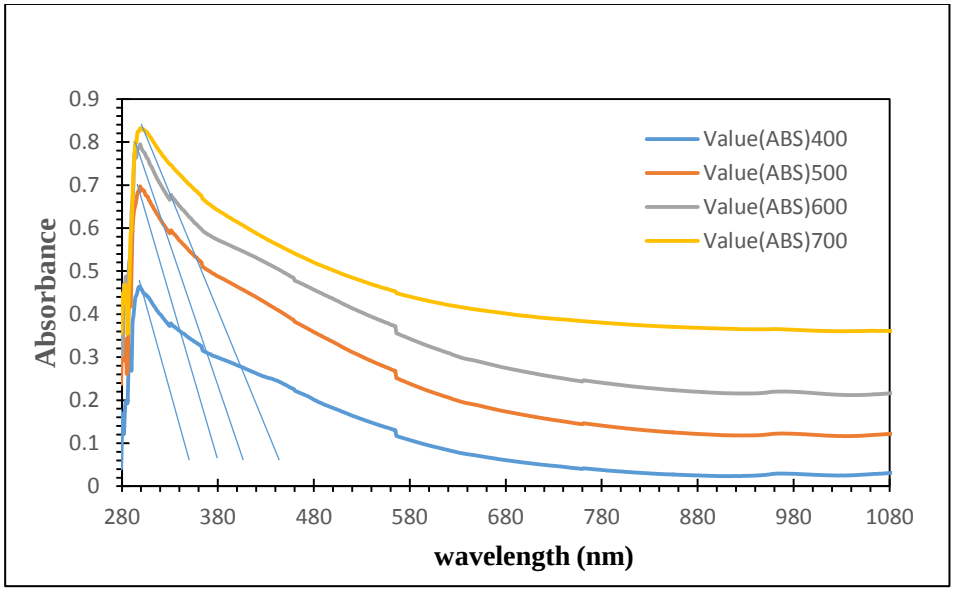

Figure 3: Shows the absorbance spectrum as a function of the wavelength of the SnO NPs with different laser energy.

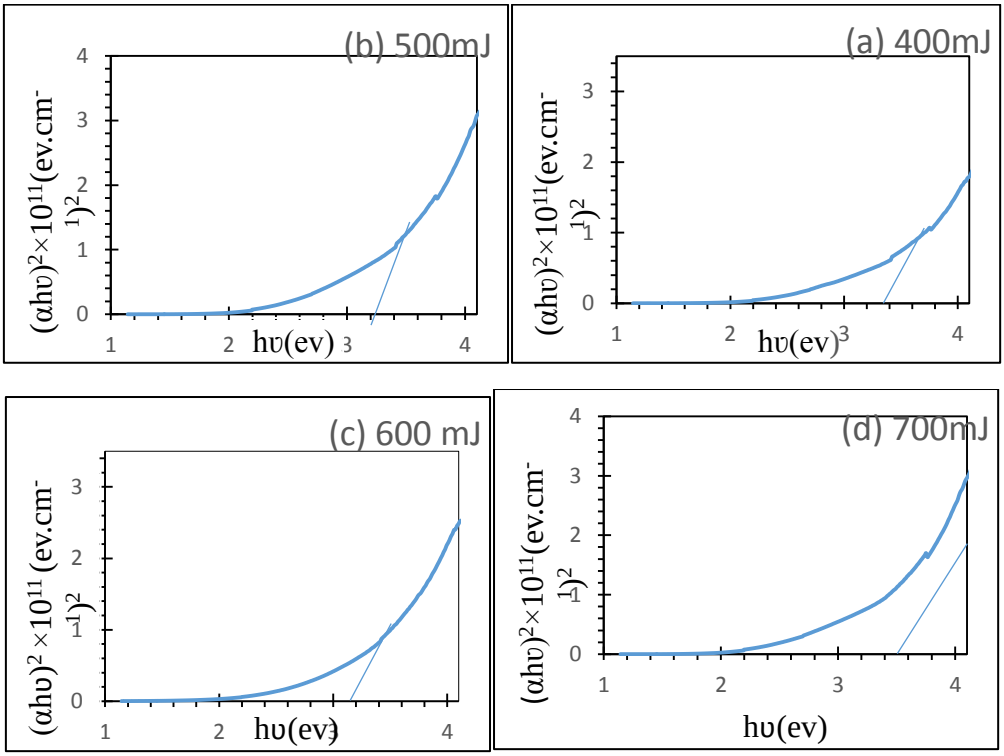

Figure 4: Shows the relationship of (αhv) 2 as a function of the photon energy of the SnO NPs prepared by laser ablation with different laser energy.

3. Atomic Force Microscope Analysis (AFM)

It is a microscopic technique that can distinguish particles on a sub-nanometer scale. In contrast to standard microscopic approaches, the AFM method visualizes the specimen by contouring its surface by regulating the stresses between a tiny and sharp probe or tip and the surface of the specimen [16]. Figure 5 displays three-dimensional images , which shows irregular surface or circular shape with homogeneous membrane. The average diameter was

(245nm), the average roughness wa(1.97 nm), and the root mean square was (1.73nm); it is clear from the results that the particle size of all atoms was in the nanoscale range.

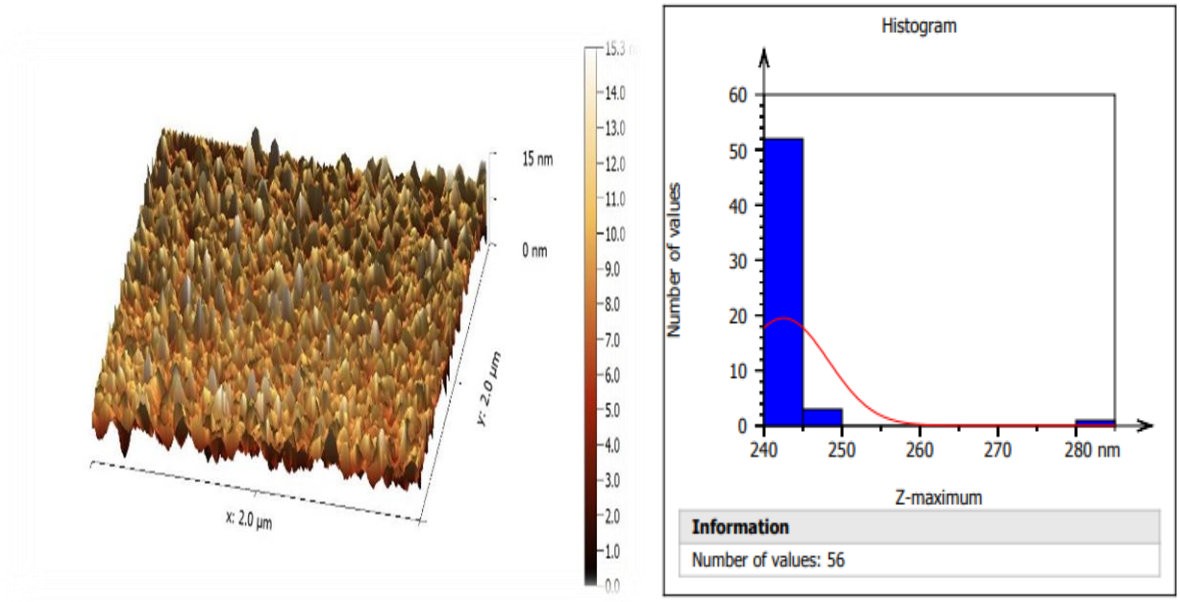

Figure 5 (a): AFM for SnO NPs prepared by PLA with 700 mJ laser energy And **(b)** granularity accumulation distributio

4. Scanning Electron Microscopy (SEM) and Energy Dispersive X-Ray Spectroscopy (EDS) or (EDX).

Scanning electron microscopy (SEM) is an essential instrument for the characterization of nanoscale materials. The scanning electron microscope (SEM) can achieve spatial resolutions of less than one nanometer because it uses electrons rather than photons for imaging [17]. Figure 6 shows the surface morphology of the SnO nanoparticles with a spherical shape. The SEM image shows agglomerations of SnO nanoparticles because of attractive forces between nanoparticles [18].

Energy Dispersive X-Ray Spectroscopy (EDS) is a common way to identify and measure the amount of each element in a very small sample of material. In a properly equipped SEM, the atoms on the surface are excited by the electron beam, causing them to emit X-rays that are characteristic of the atomic structure of the elements [19]. Figure 7 shows the presence of oxidized Tin in the sample.

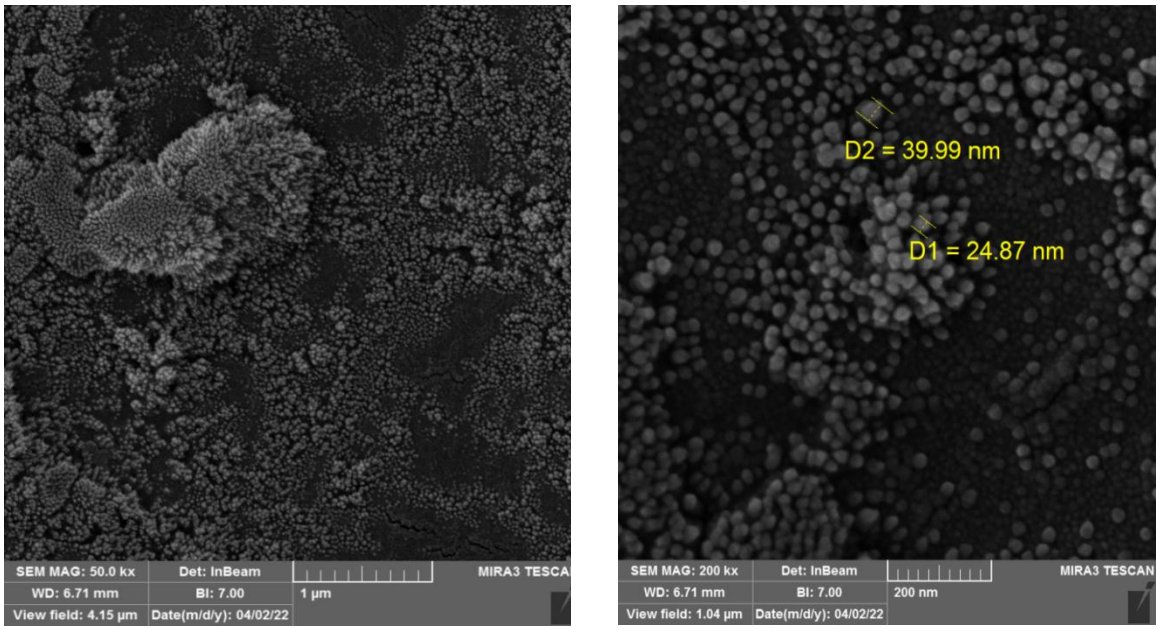

Figure 6: FE-SEM images of SnO NPs measurement at range (200nm and 1 µm) with laser energy 700mJ**.**

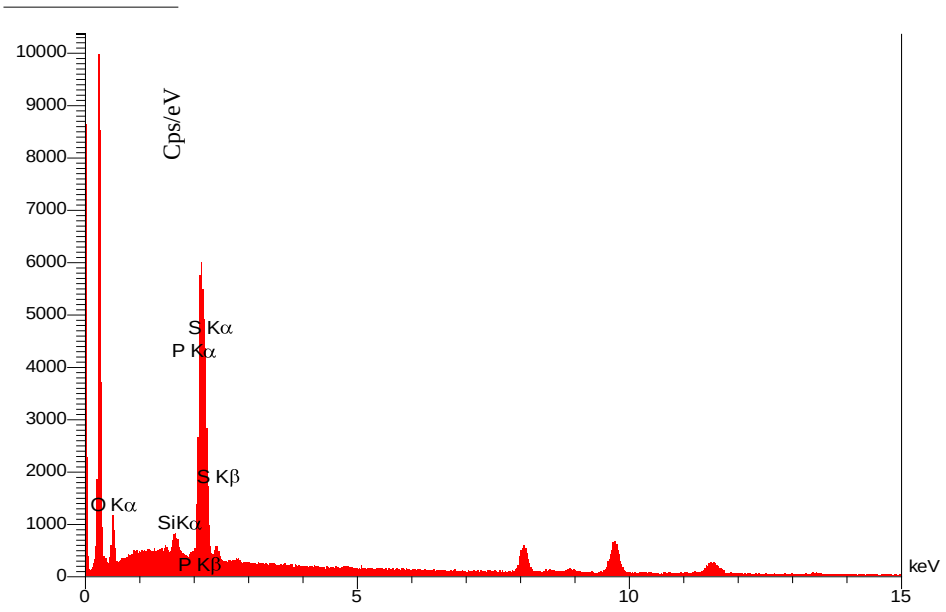

Figure 7: The EDX pattern of SnO NPs at 700 mJ laser energy.

5. Antibacterial Activity of SnO NPs.

The effect of SnO nanoparticles produced by pulsed laser ablation on the activity of gram-positive bacteria Staphylococcus aureus isolated from the ear, used nutrient agar plate cultured by striking method was investigated.The count number of bacteria before treatment was (390×10^8 colony/ml). While after treatment the count number was (170×10^8 colony/ml) using energy laser (400mJ), (41×10^8 colony/ml) with laser energy (500mJ), (20×10^8 colony/ml) with laser energy (600mJ) and zero in energy (700mJ) with Sn NPs concentration of (29.5652 ppb). From the results, it was concluded that the best laser energy to kill the bacteria was (700mJ). Figure 8 represents the proportion of bacteria before treatment and the percentage killing after treatment with the different laser energies. Staphylococcus aureus has many resistance mechanisms to survival, which are the resistance of the outer membrane

permeability to antibiotics or nanoparticles is caused by a decrease in membrane permeability and ultimately results in a reduction of drug intake. Also, efflux systems play a role in resistance to multiple drugs and this is induced by exposure for a long time to substrates present in the environment. Efflux system-encoding genes are activated and expressed, and the ability to efflux drugs is greatly enhanced, thus leading to drug, excessive production of -Lactams to anthelmintic resistance. The acquisition of a nonnative gene that codes penicillin-binding protin (PBP2a) that has a considerably lower affinity for beta-lactam antibiotics is what confers resistance on the organism. This resistance makes it possible for the process of cell-wall production, which β-lactam antibiotics are designed to block, to proceed even in the presence of ordinarily inhibitory quantities of antibiotics[20].

Figure 9 shows that bacterial growth was not affected phenotypically by the laser energies of (400, 500 and 600 mJ) but with (700mJ) laser energy, there was no growth of bacteria on the culture media.

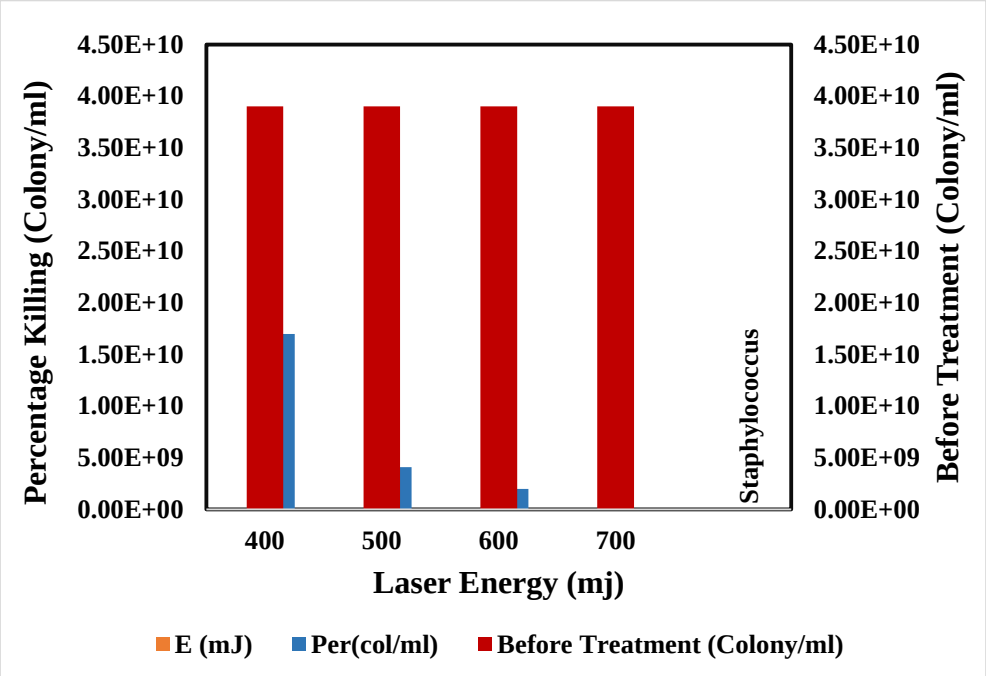

Figure 8: Histogram of antibacterial Activity at (400-700 mJ) shows the Percentage Killing.

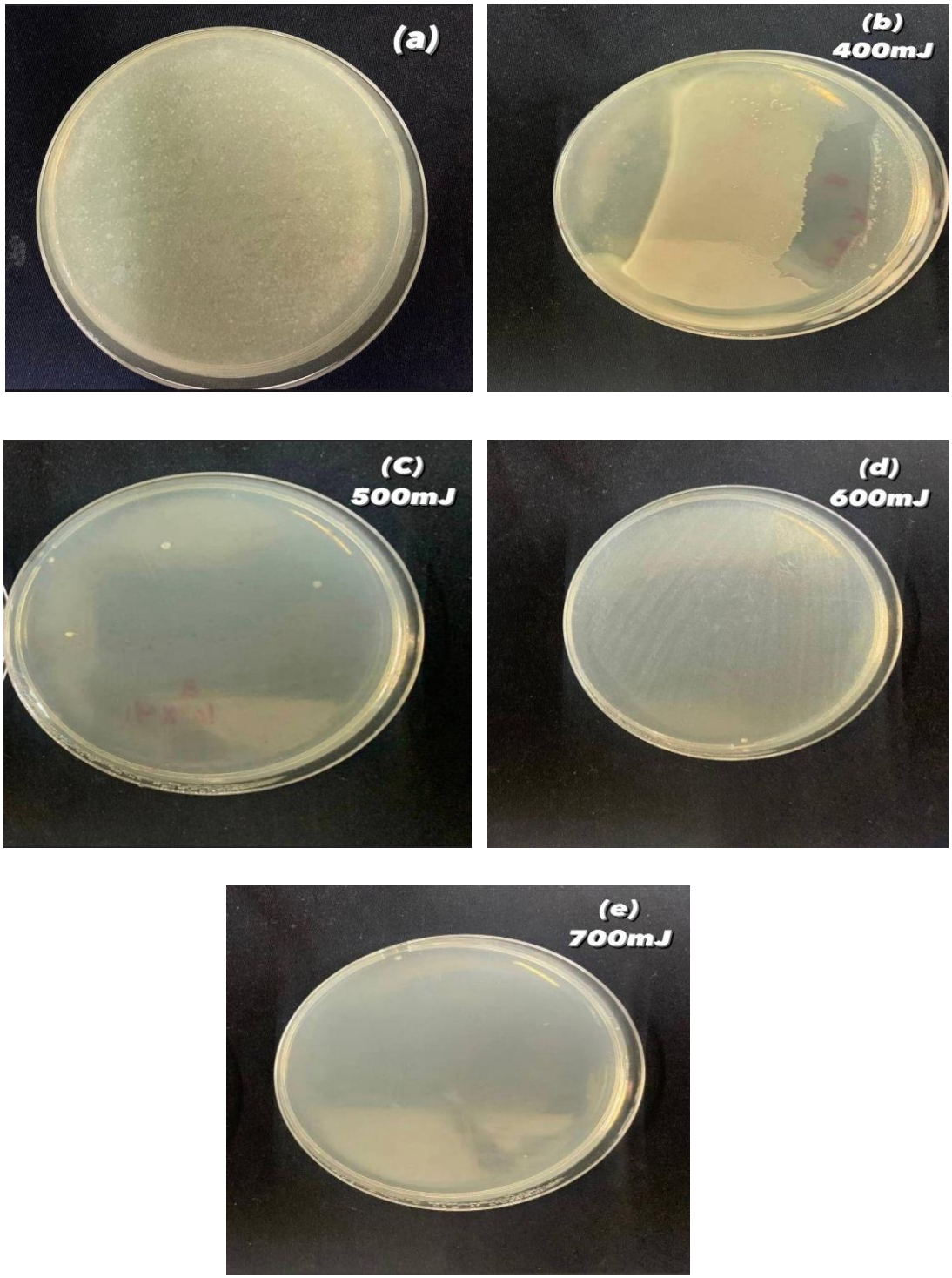

Figure 9 : Antibacterial activity *Staphylococcus aureus* at (a) Before Treatment.Aftar tretment at (b) 400 mJ (c) 500mJ (d) 600mJ (e) 700mJ

Conclusions:

An XRD analysis was carried out to detremine the structure of the tin powder before the technique was performed. Immediately following the completion of the laser-pulsed ablation technique, all of the essential procedures to identify and examine the properties of tin oxide nanoparticles were carried out. These XRD investigations are performed on tin films that were processed using the PLA technique to oxide with liquid media. The energy gap was determined by UV-Visible analysis. The energy gap was changed from (3.3eV to 3 eV) with increasing the laser energy from 400-700 Mj, respectively. The standard energy gap of tin (Sn) oxide is 3.6eV. AFM analysis showed the tin oxide samples to have high roughness, average diameter of (245nm), average roughness of (1.97 nm) and root mean square of (1.73nm). The best laser energy for completely killing the bacteria (no growth on cultured media) was 700mJ. XRD study of tin films revealed that the tin films have the ability to oxide with liquid media using the PLA approach.

Reference

[1] R. Le Harzic *et al.*, "Comparison of heat-affected zones due to nanosecond and femtosecond laser pulses using transmission electronic microscopy," *Appl. Phys. Lett.*, vol. 80, no. 21, pp. 3886–3888, 2002.

[2] Y. Dai, M. He, H. Bian, B. Lu, X. Yan, and G. Ma, "Femtosecond laser nanostructuring of silver film," *Appl. Phys. A*, vol. 106, no. 3, pp. 567–574, 2012.

[3] A. Miotello and N. Patel, "Pulsed laser deposition of cluster-assembled films for catalysis and the photocatalysis relevant to energy and the environment," *Appl. Surf. Sci.*, vol. 278, pp. 19–25, 2013.

[4] P. Hannaford, *Femtosecond laser spectroscopy*. Springer Science & Business Media, 2004.

[5] M. V Allmen and A. Blatter, *Laser-beam interactions with materials: physical principles and applications*, vol. 2. Springer Science & Business Media, 2013.

[6] N. A. Inogamov and Y. V Petrov, "Thermal conductivity of metals with hot electrons," *J. Exp. Theor. Phys.*, vol. 110, no. 3, pp. 446–468, 2010.

[7] Y. Nakata, J. Muramoto, T. Okada, and M. Maeda, "Particle dynamics during nanoparticle synthesis by laser ablation in a background gas," *J. Appl. Phys.*, vol. 91, no. 3, pp. 1640–1643, 2002.

[8] H. Wang, J. Zhang, and H. Yu, "Elemental selenium at nano size possesses lower toxicity without compromising the fundamental effect on selenoenzymes: comparison with selenomethionine in mice," *Free Radic. Biol. Med.*, vol. 42, no. 10, pp. 1524–1533, 2007.

[9] C. Jenul and A. R. Horswill, "Regulation of Staphylococcus aureus virulence," *Microbiol. Spectr.*, vol. 7, no. 2, pp. 2–7, 2019.

[10] N. K. Abdalameer, S. N. Mazhir, and K. A. Aadim, "The effect of ZnSe Core/shell on the properties of the window layer of the solar cell and its applications in solar energy," *Energy Reports*, vol. 6, pp. 447–458, 2020.

[11] Y. Shadangi, V. Shivam, M. K. Singh, K. Chattopadhyay, J. Basu, and N. K. Mukhopadhyay, "Synthesis and characterization of Sn reinforced Al-Cu-Fe quasicrystalline matrix nanocomposite by mechanical milling," *J. Alloys Compd.*, vol. 797, pp. 1280–1287, 2019.

[12] S. Tazikeh, A. Akbari, A. Talebi, and E. Talebi, "Synthesis and characterization of tin oxide nanoparticles via the Co-precipitation method," *Mater. Sci.*, vol. 32, no. 1, pp. 98–101, 2014.

[13] F. S. Rocha, A. J. Gomes, C. N. Lunardi, S. Kaliaguine, and G. S. Patience, "Experimental methods in chemical engineering: Ultraviolet visible spectroscopy—UV-Vis," *Can. J. Chem. Eng.*, vol. 96, no. 12, pp. 2512–2517, 2018.

[14] K. A. Aadim, R. A. Alansary, and S. A. Alhady, "Effect of Mn concentration on the structural and optical properties of SnO2 thin films prepared by pulse laser deposition," *IOSR J. Res. Method Educ.*, vol. 4, no. 4, pp. 12–19, 2014.

[15] K. D. Mahmood, K. A. Aadim, and M. G. Hammed, "Effect of the Pulsed Laser Energy on the Properties of CdO: NiO Composite Thin Films for Solar Cell Applications," *Iraqi J. Sci.*, pp. 1004–1017, 2022.

[16] J. Wang and S. Nie, "Application of atomic force microscopy in microscopic analysis of

polysaccharide," *Trends Food Sci. Technol.*, vol. 87, pp. 35–46, 2019.

[17] K. de Haan, Z. S. Ballard, Y. Rivenson, Y. Wu, and A. Ozcan, "Resolution enhancement in scanning electron microscopy using deep learning," *Sci. Rep.*, vol. 9, no. 1, pp. 1–7, 2019.

[18] R. S. Mohammed, K. A. Aadim, and K. A. Ahmed, "Synthesis of CuO/ZnO and MgO/ZnO Core/Shell Nanoparticles with Plasma Gets and Study of their Structural and Optical Properties," *Karbala Int. J. Mod. Sci.*, vol. 8, no. 2, pp. 88–97, 2022.

[19] Y. Chen, C. Zuo, Z. Li, and A. Chen, "Design of ceria grafted mesoporous silica composite particles for high-efficiency and damage-free oxide chemical mechanical polishing," *J. Alloys Compd.*, vol. 736, pp. 276–288, 2018.